06

Multiscale structures based on nanomaterials for the development of passive and active implantable devices that stimulate nerve tissue

© D.T. Murashko,[1] K.D. Efremova,[2] B.M. Putrya,[1] E.M. Eganova,[3] A.Yu. Gerasimenko[1,2]

[1] Institute of biomedical systems, National Research University ≪MIET≫,
124498 Moscow, Zelenograd, Russia
[2] Institute for Bionic Technologies and Engineering, Sechenov First Moscow State Medical University, Sechenov University,
119991 Moscow, Russia
[3] Institute of Nanotechnology of Microelectronics of the Russian Academy of Sciences,
119334 Moscow, Russia
e-mail: skorden@outlook.com

Received December 15, 2025
Revised December 15, 2025
Accepted December 15, 2025

This study presents the creation of multiscale structures based on nanomaterials for the fabrication of passive and active implantable devices that stimulate neural tissue through the use of laser microstructuring and carbon nanotube coatings. Results of surface morphology studies revealed the formation of a distinctly ordered surface with protruding vertical arrays and depressions. The greatest height of the arrays, in the range of 55–72 μm, was achieved in the sample irradiated with a laser power of 5.7 W. Scanning electron microscopy also confirmed the formation of a uniform coating of single-walled carbon nanotubes. Energy-dispersive X-ray spectroscopy confirmed the expected increase in oxide phases when laser radiation was used in air. At the same time, the application of a nanotube coating led to the expected increase in carbon content on the sample surfaces. A study was conducted on the effect of laser irradiation and nanotube coating on the electrical conductivity of the samples. During cyclic voltammetry, the expected response was obtained, showing that the control sample exhibited no catalytic activity compared to the other samples. The sample irradiated with 4 W laser radiation and coated with single-walled nanotubes exhibited the highest combination of cycle stability (98.7 %) and areal capacitance 125.7 μF/cm^2.

Keywords: carbon nanotubes, medical-grade steel, laser radiation, multiscale structures, neurostimulation.

DOI: 10.61011/TP.2026.05.63518.332-25

Introduction

Implantable neurostimulators are a rapidly growing sector of biomedical devices that are dealing with issues of impaired motor activity, neurological and sensory impairments. One of the key elements of such devices is the electrode–-tissue interface expected to provide effective charge transfer between the device and the nervous system. However, conventional materials are not capable of providing high electrochemical activity, mechanical and corrosion resistance at the same time [1–3]. For instance, conventional materials for implantable electrodes, such as platinum and its alloys, are featuring high corrosion resistance and have proven themselves well in medical practice, however, these materials have a low ability to accumulate the charge and electrochemical activity due to the lack of a developed surface and low contact area [4,5].

A promising direction for improving the electrophysical characteristics of electrodes is the use of laser methods for surface micro-structuring. Such laser processing allows to form hierarchical micro- and nanostructures, providing a multiple increase in the working surface area without using additional materials [6,7]. This modification of the surface leads to a significant decline in impedance and an increase in charge storage capacity due to formation of vertical arrays that contribute to the involvement of a larger number of active sites [8].

At the same time, active research is underway in the field of integrating the carbon nanotubes (CNT) as a conductive material for electrode modification. CNT tubes are well-known to boast an outstanding combination of high electrical conductivity, specific surface and mechanical characteristics, which potentially makes their use promising for the formation of a biomimetic interface between the electrode surface and the nervous tissue. The use of CNT makes it possible to achieve a lower impedance, higher charging capacity and improved quality of the neural activity registration [9–11].

Given the above, it makes sense to focus on the research aimed at creating multi-scale structures that combine the benefits of the laser-induced microstructures and integrated CNT. This approach allows to combine a mechanically stable microrelief base with a high specific surface area of CNT, while providing low impedance and high charge capacity [12,13].

The present study is focused on fabrication of the multiscale nanomaterial structures to create passive and active implantable devices that stimulate the nerve tissues and are formed due to the effects of laser micro-structuring and subsequent introduction of carbon nanotubes. The main focus is on the study of morphological characteristics, changes in elemental composition, electrical and electrochemical characteristics.

1. Materials and research methods

1.1. Formation of nanomaterial multiscale structures for the fabrication of passive and active implantable devices stimulating the nerve tissue

Samples of the multi-scale structures based on nanomaterials for the fabrication of passive and active implantable devices that stimulate the nerve tissue were formed on plates made of medical steel AISI 316L. The components of this steel grade are listed in Table 1 below.

The steel was cut in rectangular plates $20 \times 10 \times 1$ mm in size. To form the nano-scale structures on the plates surface the single-walled carbon nanotubes (SWCNT) („Universalnie Dobavki“, Novosibirsk, Russia) were used. For their use, a dispersed medium — a liquid base — was prepared, from which a layer of SWCNTs was formed. Distilled water was used as a solvent. To achieve homogeneity of the dispersed medium, the surfactant sodium deoxycholate was used. The concentration of the dispersed medium components was 0.1/0.9 mg/ml for SWCNT and sodium deoxycholate, respectively.

The formation of a microstructure on the plate surface was provided by exposure to laser radiation. The microstructures were formed by means of a pulsed ytterbium fiber laser with a wavelength of 1064 nm, pulse duration of 100 ns, laser beam speed of 100 mm/s, frequency of 25 kHz and laser radiation power in the range of 3.5–7.3 W. After the formation of the microstructural surface, the plate was cleaned to remove ablation products. The cleaning process included ultrasonic treatment of the plates sequentially in acetone, ethyl alcohol and distilled water, for 10 min in each solvent. Next, a layer of SWCNT was applied to the formed microstructured surface. To improve adhesion, the surface was treated with ultraviolet radiation. SWCNT were applied using the sputtering method and heated plates using a heating table. The table was heated to a temperature of 70 °C. The dispersed medium was applied layer by layer by using a three-coordinate sputtering system. Dispersed medium supply pressure was equal to 2 bar. A total of 200 layers were deposited. The resulting SWCNT layer was ($\sim 500 \pm 100$) nm thick. A schematic representation of the formation of multiscale structures is shown in Fig. 1.

Table 1. Components of steel AISI 316L

Carbon (C): ≤ 0.03 %	Mangenese (Mn): ≤ 2 %
Chromium (Cr): 16 %–18.2 %	Silicon (Si): ≤ 1.0 %
Nickel (Ni): 10.1 %–14.1 %	Phosphorus (P): ≤ 0.045 %
Molybdenum (Mo): 2 %–3 %	Sulfur (S): ≤ 0.03 %

The following kinds of samples were studied:

1) a plate made of AISI 316L steel was used as a control specimen;

2) steel plates with a microstructured surface resulting from exposure to laser radiation;

3) steel plates with a multiscale surface structure based on nanomaterials.

1.2. Scanning electron microscopy and energy dispersive X-ray spectroscopy

The structural features of samples of nanomaterial multiscale structures used in fabrication of passive and active implantable devices stimulating the nerve tissue were studied using scanning electron microscopy (SEM) on FEI Helios NanoLab650 microscope (FEI Ltd., Hillsboro, OR, USA). The accelerating voltage of the electron column was 5 kV, the current of the electron probe was 50 pA for the control sample, the sample with a microstructured surface and samples with a multiscale surface structure. Vacuum chamber pressure was $1.9 \cdot 10^{-3}$ Pa. Samples were attached to a conducting substrate using carbon adhesive tape. Energy dispersive X-ray spectroscopy (EDX) was performed using Bruker Quantax XFlash 6 system with a modular backscattered electron diffraction system in a vacuum chamber of an electron microscope.

1.3. Optical profilometry

The morphological changes in the surface of the sample obtained as a result of exposure to pulsed laser radiation were evaluated using S Neox optical profilometer. S Neox profilometer is fitted with a motorized lens-turret for five interchangeable lenses: 10X, 20X, 50X, 100X, 150X. Maximal resolution of the profilometer in Z axis was 0.5 nm. The range of measurements along Z axis has different values depending on the mode used: PSI (Phase Shift Interferometry) up to 20 μm; CSI (Coherent Scanning Interferometry) — up to 10 mm; confocal mode — up to 34 mm.

During the experimental study, the confocal profilometer mode was used to analyze the surface topography of the samples. At the first stage, confocal microscopy was performed using a 50X lens, resulting in high-contrast $2D$ images of the studied samples' surface in optical mode.

The measurements were organized as follows: The studied sample was fixed on a motor-driven table of the microscope providing the sample's precision movement in XY plane with a positioning accuracy of several micron. With the help of the built-in software and video guidance system, a specific area of the surface was selected for subsequent scanning. Before scanning each individual cell, the autofocus function was automatically activated, which ensured accurate collection of data on the relief of the samples. To ensure seamless data integration and construction of a continuous topographic map of a large area, the scanning was performed with 10 % overlap of

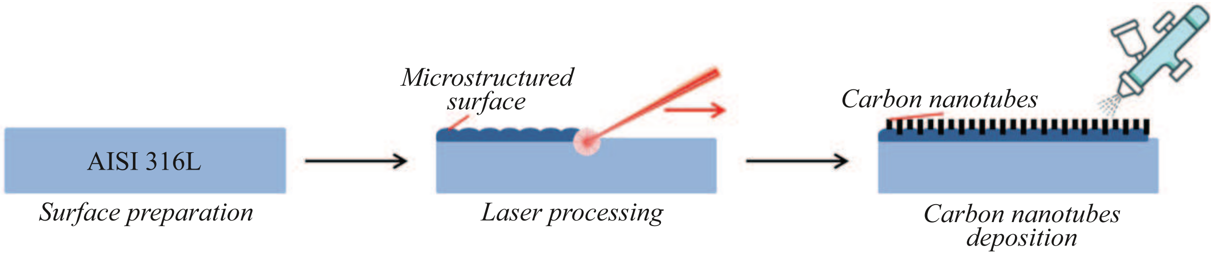

Figure 1. Formation of nanomaterial multiscale structures for the fabrication of passive and active implantable devices that stimulate the nerve tissue.

adjacent fields of view. The collected data was processed using embedded software that allows visualization and analysis of the obtained 2D surface sections (linear profiles). The linear profile was taken diagonally across the area of the studied sample.

1.4. Electric conductivity measurement

The conductivity was measured using a four-probe measuring unit (JG ST-2258C, Jingle Electronics Co., China) as follows: first, the geometry of the studied samples was defined; the measured dimensions were entered into the dedicated software, which calculated the calibration parameters for the measuring unit based on the data; after entering the calibration parameters, the studied samples were placed on a slide table; finally, the measuring probes were inserted into the center of the samples, after which the resistivity values (ρ) were registered. The found values were recalculated to obtain electric conductivity (σ), and after that they were averaged.

1.5. Cyclic voltamperograms study

To study the electrochemical properties of samples of multiscale nanomaterial structures for fabrication of passive and active nerve tissue stimulating implantable devices, an electrochemical cell, a voltammetry stand, and Python software for processing the potentiodynamic characteristics were used. This software package allows to study the electrochemical properties of the multiscale nanomaterial-based structures, evaluate the stability and capacitance characteristics of electrodes, and automate the stages of experimental data processing. The developed program combines the functions of downloading cvs files, automatically determining the structure of the downloaded table and units of measurement, and highlighting the existing individual cycles. The interface has an option of displaying the current versus voltage curves, selecting a range for calculations, and interacting with the download data series. The program allows you to calculate the values of the anode and cathode charges, the area capacity both through the integral and through the normalization of the scan rate, as well as the capacitance stability.

The study was conducted using cyclic voltammetry method [14] with the help of a potentiostat-amperostat PI-50-Pro. This potentiostat-amperostat is designed for studying the liquid and solid-state systems. For basic measurement methods, it is possible to change the operating parameters of the device during the experiment, which allows to enhance the control over the system during measurements.

A three-electrode connection diagram was used to study the electrical activity of samples of the multiscale nanomaterial structures designed to fabricate passive and active nerve tissue stimulating implantable devices. In this diagram, the potential between the working electrode and the reference electrode is measured, and the reference electrode is brought as close as possible to the working electrode, thus minimizing ohmic losses during the experiment. The potentiodynamic curves were registered in an electrochemical cell, the schematic representation and general view of which are shown in Fig. 2.

The electrochemical cell is made of a borosilicate glass. The cover of the electrochemical cell is ground at the junctions with the cell to ensure the system tightness. The cover has five inputs for argon supply, a buffer solution supply system for pH stabilization, an auxiliary electrode and a salt bridge connecting the reference electrode to the working electrode.

To bring the surface of the working electrode to the electrochemical cell, a lifting table is provided, which ensures tight contact of the working electrode with the cell. Pressing electrodes made of copper are provided to connect the working electrode to the potentiostat.

A platinum mesh placed in a glass container with a Schott filter was used as an auxiliary electrode. The auxiliary electrode is placed in a separated space container because of the need to separate the electrolysis products of the solution components of the working and auxiliary electrodes, as well as to exclude the impact of compounds obtained on the auxiliary electrode on the nature of cyclic voltammograms.

The silver-chlorine half-cell Ag/AgCl was used as a reference electrode. The silver-chlorine half-cell was placed in a separate container filled with a saturated solution (3M) of potassium chloride.

A phosphate-salt buffer with a hydrogen value pH of 7.26 was used as a standardized test solution. The rationale is

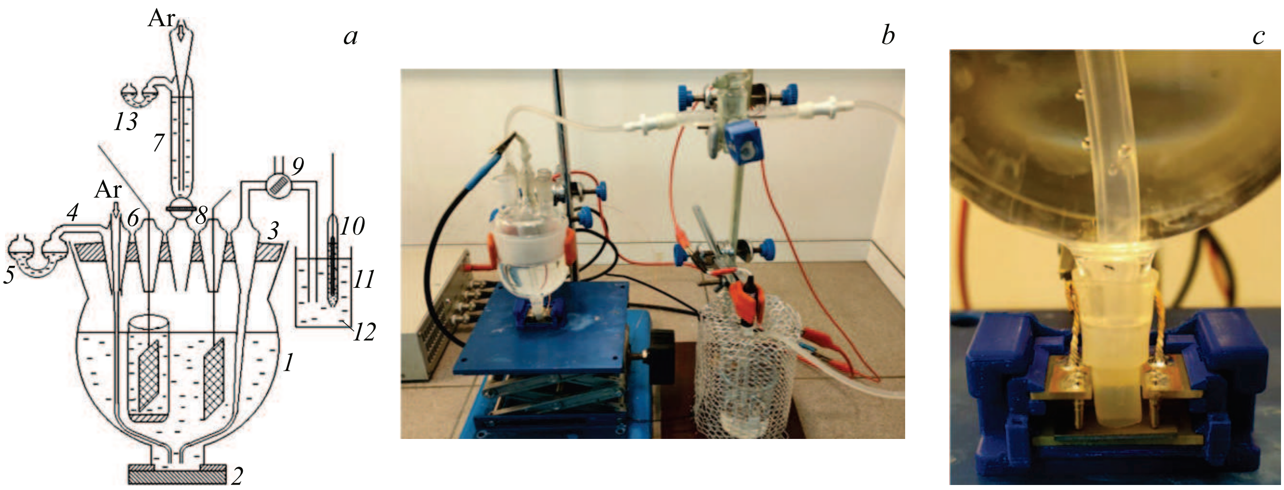

Figure 2. Schematic representation (*a*) an general view (*b*) of an electrochemical cell, general view of the studied sample in the holder (*c*): *1* — glass body of the electrochemical cell; *2* — contact clamps; *3* — cover of the electrochemical cell; *4* — argon blowing inlet; *5* — water lock; *6* — auxiliary electrode with a separated space; *7* — buffer solution; *8* — test platinum electrode; *9* — salt bridge; *10* — silver-chlorine half-cell Ag/AgCl; *11* — cell with a saturated KCl solution; *12* — enriched with KCl solution; *13* — water solution.

as follows: the standardized test solution was supposed to simulate the environment of the spinal cord, with its hydrogen index in the range of 7.2−7.4. The hydrogen index may impact the nature of cyclic voltammograms, therefore, a fixed pH value in indicated values was pivotal in the experiments.

2. Experiment

2.1. Analysis of changes in the surface morphology of the multiscale nanomaterial structures used in fabrication of passive and active nerve tissue stimulating implantable devices

Figure 3 shows a SEM image of the surface, 3*D* surface profile, and a profilogram of a sample obtained by irradiation with 3.5 W laser.

The analysis of the surface morphology after exposure to laser radiation showed formation of a regular relief with a pronounced periodicity. In SEM image, one can observe a number of vertically oriented arrays that line up in an ordered grating. Such a frequency may indicate a stable exposure of the substrate material to laser radiation, when a local melting occurs. The data obtained during profilometry confirm the formation of a pronounced relief with height differences of the order of tens of micrometers. The dimensions of the vertical arrays, based on the obtained profilograms, are 35−37 μm in height and 50−60 μm in diameter. The approximate size of the recess on the sample surface is in the range of 15−18 μm. Holes inside the arrays themselves are also visible on the surface of the arrays of this sample, presumably obtained as a result of exposure to laser radiation pulses. The presence of spherical particles formed during local melting as a result of laser exposure to [15] is observed.

The presence of such vertically oriented arrays and recesses contributes to an increase in the surface area of the samples, which, in turn, results in a higher working surface of the neurostimulating electrodes. Such a surface also makes it possible to improve the capacitive characteristics of the electrodes, which is an important condition in the neurostimulators design.

Figure 4 shows a SEM image of the surface, 3*D*-profile of the surface, and a profilogram of a sample obtained by irradiation with 4.0 W laser.

Further studies of the surface morphology with increasing laser radiation power demonstrate the further development of the surface. SEM-image shows that regular character of vertical arrays is preserved, while the arrays themselves become more pronounced. No holes in the center are visible on the surface of the vertical arrays. The height of the obtained arrays stays within the range of 35−40 μm, diameter — within the range of 52−60 μm. The approximate recess diameter makes 11−14 μm. Similarly, the presence of spherical metal particles on the surface of the arrays is observed. The results show a slight increase in the height and diameter of the arrays. These changes indicate a slight increase in the arrays' height and diameter.

Figure 5 shows a SEM image of the surface, 3*D*-profile surface, and a profilogram of a sample exposed to a laser with a power of 4.6 W.

As a result of further exposure to laser radiation, the morphology of the surface remains regular, but there is a change in the shape of the arrays. It can be seen from these images that the shape of vertical arrays after exposure to laser radiation with a power of 4.6W becomes more elongated, having a more conical shape. Examination of the surface profile shows an increase in the amplitude of

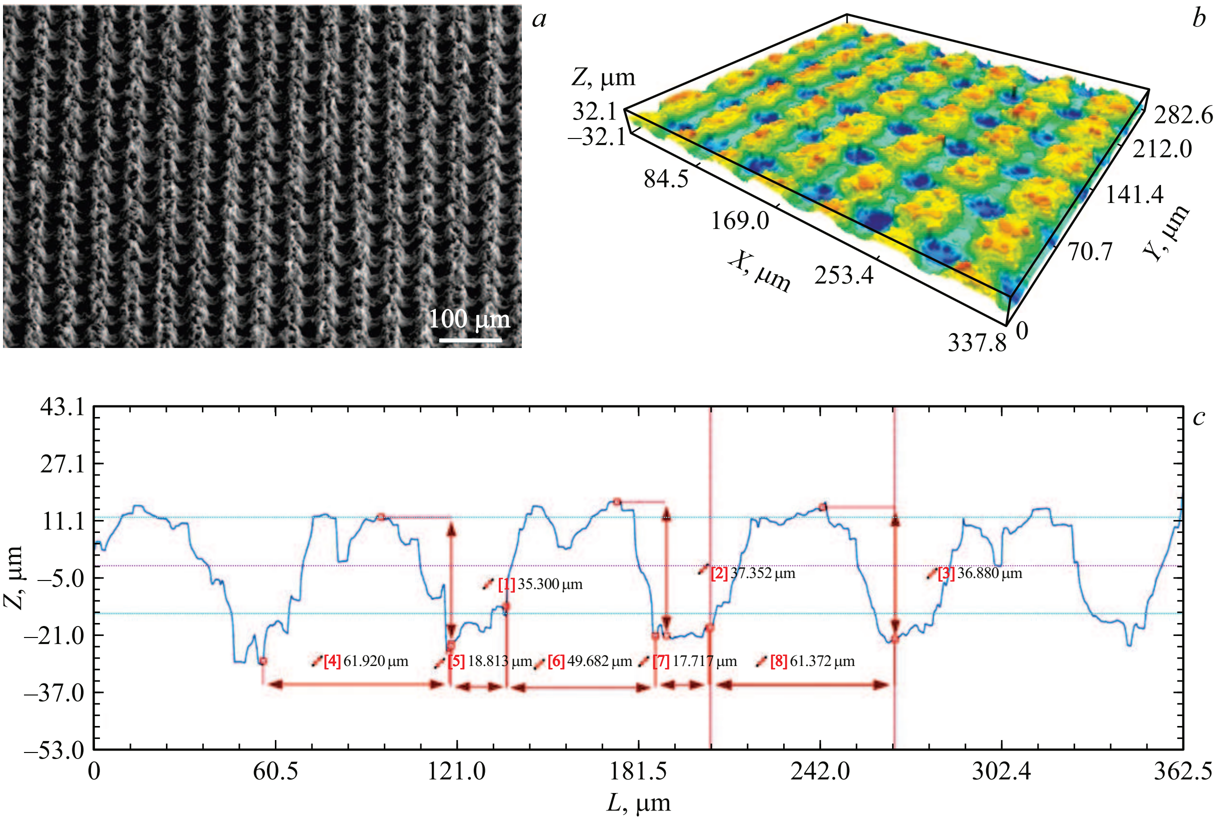

Figure 3. Morphology of the surface of a sample irradiated by laser with a power of 3.5 W; *a* — SEM image of the surface, *b* — 3*D* surface profile, *c* — surface profilogram.

height differences, where the maximum values are shifted upward, while at the same time maintaining the minimum values. Height of the obtained arrays lies within the range 36–52 μm, and their diameter — 45–66 μm. The diameter of the depressions remains approximately similar to the previous samples and is in the range of 14–20 μm. Thus, the continued repeatability of the surface morphology indicates the stability of the formation mechanism with increasing laser radiation power.

Figure 6 shows a SEM image of the surface, 3*D*-surface profile, and a profilogram of a sample obtained by irradiation with a 5.1 W laser.

From the images obtained, it can be seen that the vertical arrays have a more uniform cone-shaped shape compared to the previous samples. The presence of spherical particles obtained as a result of laser ablation is mentioned. However, it should be noted that these particles are more shifted to the tops of the arrays than to their sides. A pattern remains where, with increasing laser radiation power, the geometry of vertically oriented arrays increases. The arrays height remains in the range 46–65 μm, and their diameter makes 42–66 μm. The recess width is 20–23 μm.

Figure 7 shows a SEM image of the surface, 3*D*-profile of the surface, and a profilogram of a sample obtained after the sample irradiation with a 5.7 W laser.

Analysis of the morphology of the sample showed a decrease in the amplitude of height differences in the vertically aligned arrays. The SEM image indicates that periodicity of the structure remains, but the vertical arrays themselves no longer undergo significant changes. Based on the images obtained, it can be concluded that the vertical arrays retain a uniform shape. Also, a reduction in height differences of vertical arrays compared to previous samples should be mentioned. The height of the arrays was 55–72 μm, diameter of the arrays — 40–65 μm. Diameter of the recess was 24–26 μm.

Based on the data from the studied samples, it can be concluded that with increasing laser power, the arrays will become higher until a point is reached when further increase in laser radiation will not lead to pronounced changes in the shape of the arrays or its degradation. At the same time, the diameter of the vertical arrays does not undergo significant changes, amounting to a value not exceeding 65 μm.

Fig. 8 illustrates SEM images of a SWCNT coated sample.

Based on the images obtained, it can be concluded that SWCNT coating is homogeneous and completely covers the previously formed vertical arrays and depressions. At the same time, the CNT tubes themselves are not perfectly ordered: the nanotubes assemble into disoriented bundles and form a mesh-like porous structure. Formation of a SWCNT layer has a number of benefits: first, the

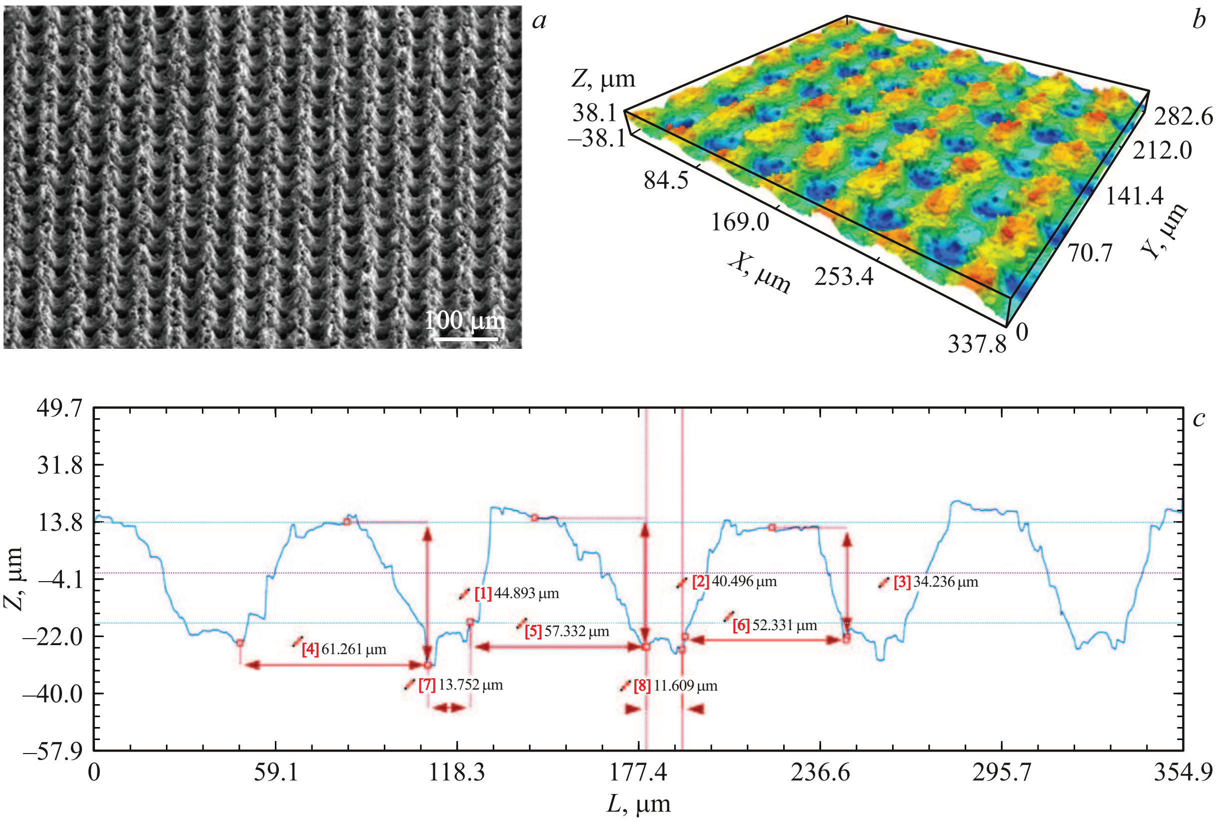

Figure 4. Morphology of the surface of a sample irradiated by laser with a power of 4 W; *a* — SEM image of the surface, *b* — 3*D* surface profile, *c* — surface profilogram.

mesh-like structure of the nanotubes greatly enlarges the electrode effective surface area directly impacting the charge injection capacity and reducing the impedance during the electrochemical tests. Secondly, the high conductivity of SWCNT ensures efficient charge transport and stable response under stimulation conditions. Finally, CNT tubes have good biocompatibility and create a softer interface compared to a metal substrate, provided they are embedded in a biopolymer matrix or functionalized [16,17]. This helps to reduce the risk of inflammatory reactions and mechanical irritation of surrounding tissues.

2.2. Energy dispersive X-ray spectroscopy

Table 2 shows EDS data of samples with a surface treated with laser radiation.

According to the obtained data, we conclude that the surface contains the main elements of AISI 316L alloy, i.e. iron, chromium, nickel and carbon. However, after exposure to laser radiation, a high content of oxide phases is also observed, which is natural when exposed to high-energy laser radiation in air. Table 3 gives EDS data for samples exposed to laser radiation and coated with SWCNT.

These results indicate a high carbon content, which is evidence of SWCNT coating formation on the surface of the samples. The occurrence of sodium is also observed, which is because of the use of sodium deoxycholate.

2.3. Conductivity of the multiscale nanomaterial structures for the fabrication of passive and active nerve tissue stimulating implantable devices

A series of tests was made to measure the conductivity of the multiscale nanomaterial structures used in fabrication of passive and active nerve tissue stimulating implantable devices. The results of conductivity measurements in samples irradiated with a 3.5–5.7 W laser are provided in Table 4.

The obtained values show that there were no qualitative changes in electrical conductivity compared to the control sample. Only minor deviations are visible, which nevertheless fall within the margin of error. Thus, exposure to laser radiation on the surface of the samples and subsequent surface cleaning have no any impact on the conductivity of samples.

Next, measurements were made of the conductivity of samples irradiated with a laser with a power in the range 3.5–5.7 W and coated with SWCNT. The measurement results are provided in Table 5.

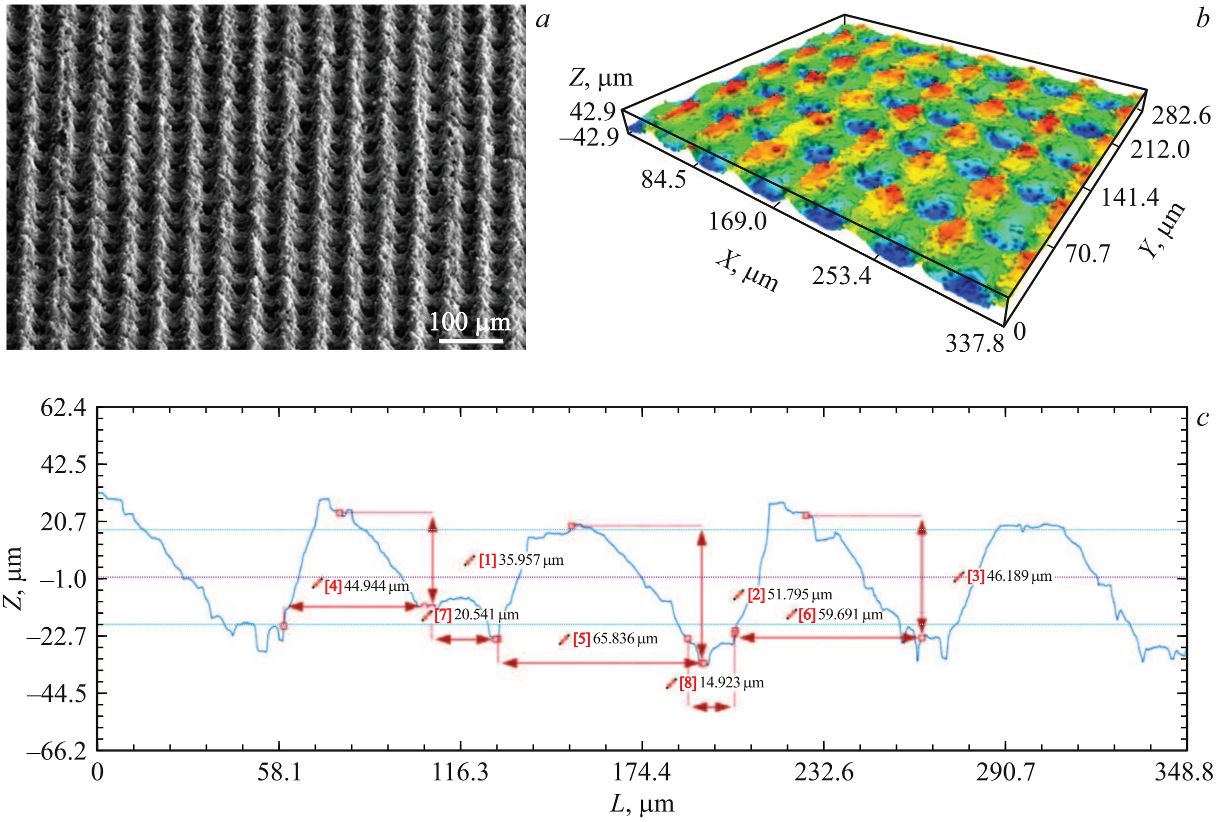

Figure 5. Morphology of the sample surface irradiated by the laser with a power of 4.6 W; *a* — SEM image of the surface, *b* — 3*D*-profile of the surface, *c* — surface profilogram.

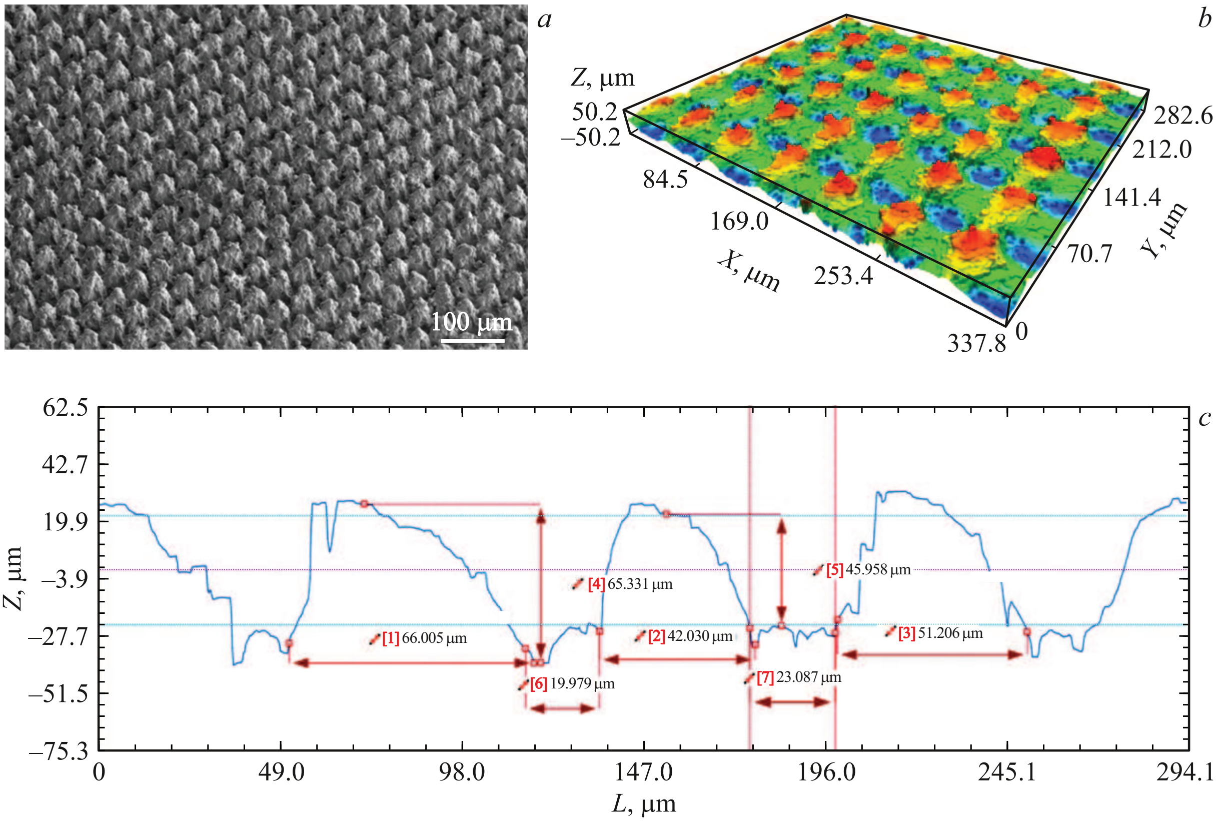

Figure 6. Morphology of the surface of a sample irradiated by laser with a power of 5.1 W; *a* — SEM image of the surface; *b* — 3*D*-surface profile; *c* — surface profilogram.

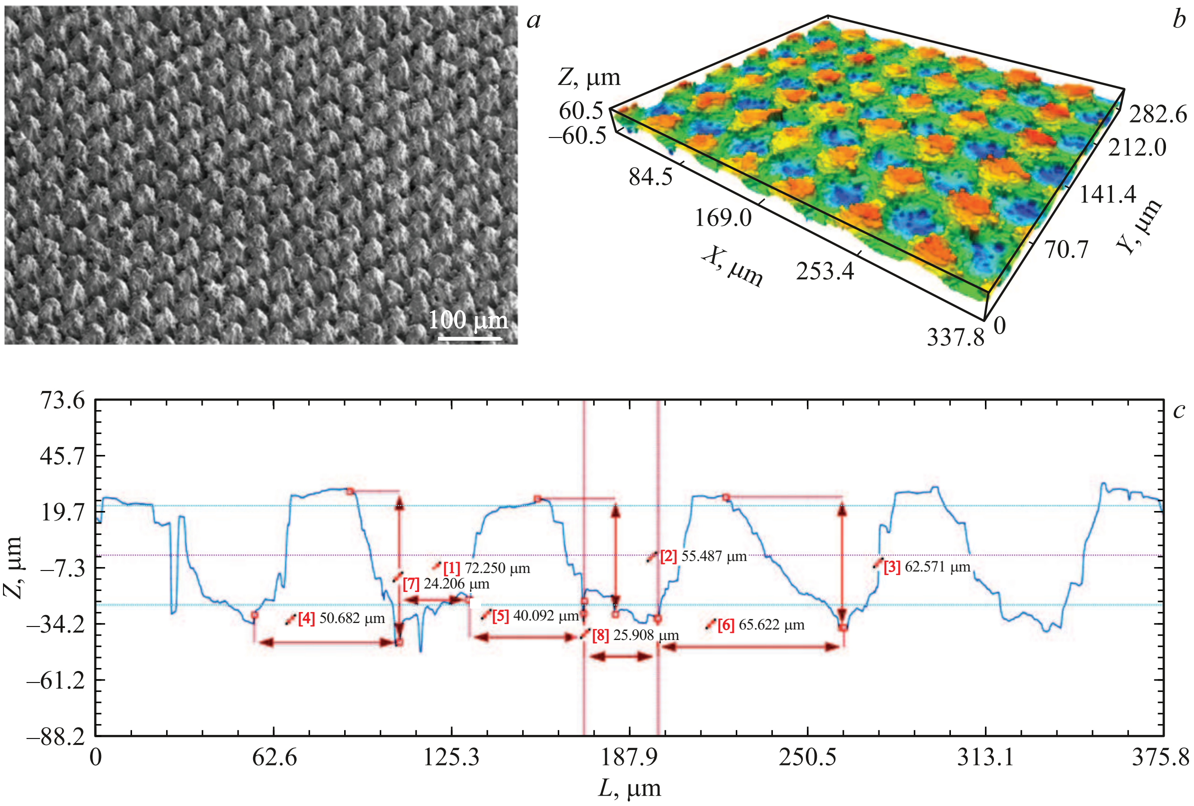

Figure 7. Morphology of the surface of a sample irradiated by laser with a power of 5.7 W; *a* — SEM image of the surface, *b* — 3*D*-profile of the surface, *c* — surface profilogram.

Based on the values obtained, it can be seen that SWCNT coating did not result in any significant changes in electrical conductivity. Moreover, all samples are comparable in values with the electrical conductivity of the control sample. Thus, having considered the influence of laser radiation and SWCNT coating on conductivity of the samples surface, it can be concluded that these factors do not have any significant effect on conductivity of the surface.

2.4. Analysis of changes in the electrochemical characteristics of the multiscale structures based on nanomaterials used in fabrication of passive and active nerve tissue stimulating implantable devices

Fig. 9 illustrates the cyclic voltammograms for the control sample, as well as for the samples of nanomaterial multiscale structures used in fabrication of passive and active nerve tissue stimulating implantable devices after laser irradiation.

It can be seen from these curves that the control sample does not exhibit any catalytic activity in the specified potential range in comparison with the rest of the samples. In case of the studied samples, it can be seen that the amplitude of the current rises under the influence of increased exposure to laser radiation. Higher values of current may be explained by the increase in the active surface with the higher rate of laser radiation. Yet, in case of a power of 5.7 W, it can be seen that the current values are lower, which may indicate possible damage to the structure. The curves themselves are the closed loops,

Table 2. EDS image of a sample of nanomaterial multiscale structures used in fabrication of passive and active nerve tissue stimulating implantable devices

Carbon (C): 14.46 at.%	Silicon (Si): 1.63 at.%
Oxygen (O): 19.97 at.%	Molybdenum (Mo): 0.52 at.%
Ferrum (Fe): 30.83 at.%	Chromium (Cr): 26.85 at.%
Nickel (Ni): 5.74 at.%	

Table 3. EDS image of a sample of nanomaterial multiscale structures used in fabrication of passive and active nerve tissue stimulating implantable devices after the sample was exposed to a laser radiation and coated with SWCNT

Carbon (C): 50.23 at.%	Silicon (Si): 0.95 at.%
Oxygen (O): 30.35 at.%	Molybdenum (Mo): 0.15 at.%
Ferrum (Fe): 8.90 at.%	Chromium (Cr): 7.90 at.%
Nickel (Ni): 0.98 at.%	Sodium (Na): 0.55 at.%

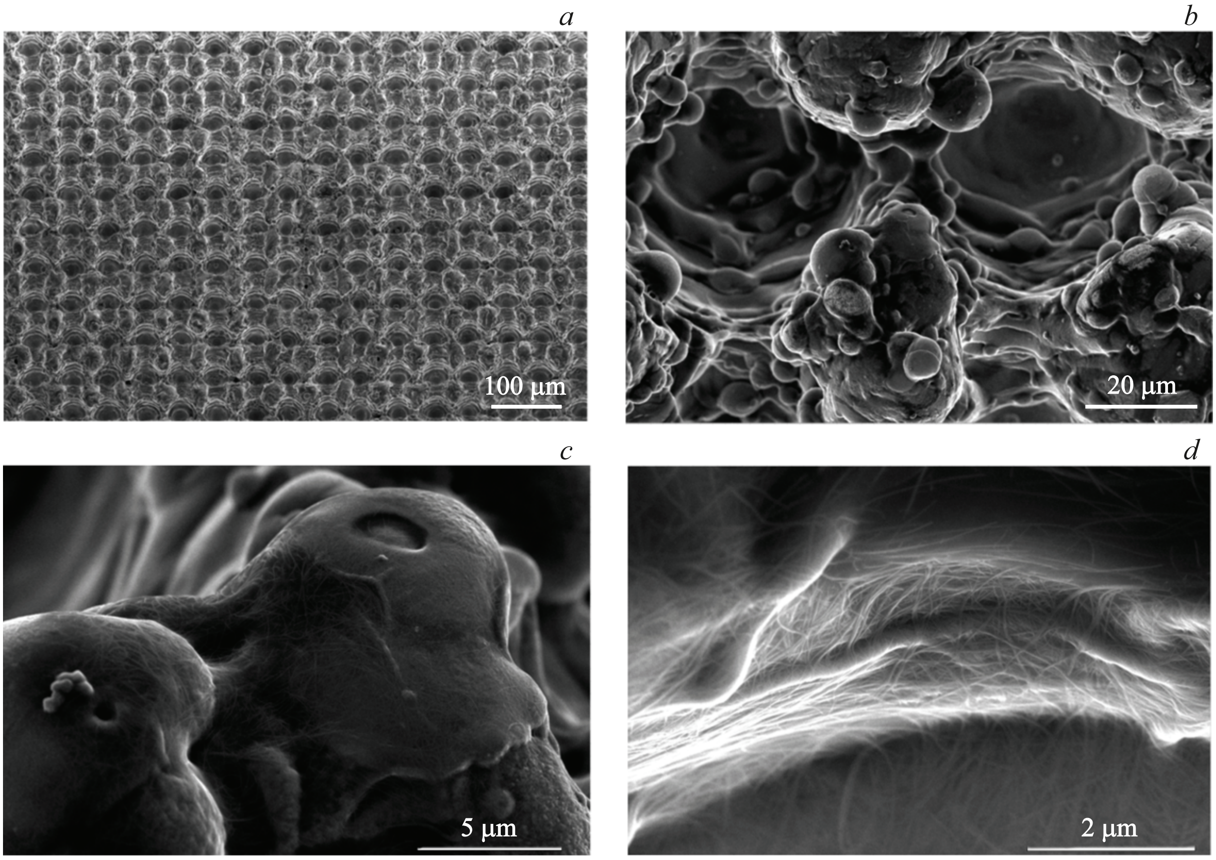

Figure 8. SEM image of samples coated with a SWCNT layer, magnified: *a* — 500x; *b* — 4000x; *c* — 20 000x; *d* — 60 000x.

Table 4. Conductivity of the samples of nanomaterial multiscale structures used in fabrication of passive and active nerve tissue stimulating implantable devices

Sample	Control	3.5 W	4 W	4.6 W	5.1 W	5.7 W
Conductivity, S/cm	16.0 ± 0.1	15.9 ± 0.4	15.8 ± 0.1	15.6 ± 0.1	16.3 ± 0.3	16.3 ± 0.2

Table 5. Conductivity of the samples of nanomaterial multiscale structures used in fabrication of passive and active nerve tissue stimulating implantable devices after exposure to laser radiation and coating with SWCNT

Sample	Control	3.5 W	4 W	4.6 W	5.1 W	5.7 W
Conductivity, S/cm	16.0 ± 0.1	16.1 ± 0.3	16.2 ± 0.2	16.0 ± 0.2	16.0 ± 0.2	15.5 ± 0.3

which indicates the capacitive pattern of the samples. The measured capacitance of the samples is shown in Table 6 below.

Judging from the obtained values, it can be concluded that the sample irradiated with a laser power of 4.6 W had the largest area capacitance. At the same time, it is worth noting that the samples irradiated by a laser of 4 and 5.7 W had the greatest stability of preserving the capacitance during the cycles.

Next, Fig. 10 shows cyclic voltammograms of samples of multiscale nanomaterial structures for creating passive and active nerve tissue stimulating implantable devices after exposure to laser radiation and deposition of SWCNT coating.

It can be seen from these curves that, as in the previous case, the voltammograms of the experimental samples differ from those in the control sample. It can also be seen that higher laser radiation power grows with the current amplitude. In this case, this is explained both by the increase in surface area caused by formation of microstructural arrays and by formation of a SWCNT layer. Moreover, it can be seen from the graphs that the current amplitude of the SWCNT-coated samples exceeds the current amplitude of the samples that were irradiated

Table 6. Capacitance of the samples of multiscale nanomaterial structures used in fabrication of passive and active nerve tissue stimulating implantable devices after laser irradiation

Sample	Control	3.5 W	4 W	4.6 W	5.1 W	5.7 W
Surface capacitance, μF/cm^2	0.79 ± 0.01	7.6 ± 0.1	17.1 ± 0.1	33.5 ± 1.6	27.7 ± 1.0	19.5 ± 0.2
Stability, %	97.2	98.2	99	85	87.4	99

Table 7. Capacitance of the samples of multiscale nanomaterial structures used in fabrication of passive and active nerve tissue stimulating implantable devices after laser irradiation and deposition of SWCNT coating

Sample	Control	3.5 W	4 W	4.6 W	5.1 W	5.7 W
Surface capacitance, μF/cm^2	0.79 ± 0.01	26.3 ± 0.4	122.7 ± 5.9	76.2 ± 1.9	85.7 ± 2.5	79.8 ± 2.1
Stability, %	97.2	99.0	98.7	91.4	91.0	91.3

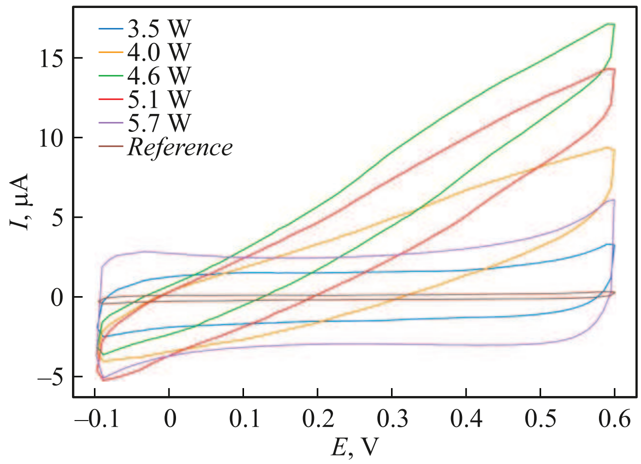

Figure 9. Cyclic voltammograms of the control sample and samples treated with laser radiation of 3.5–5.7 W power. Field scan rate — 100 % mV/s.

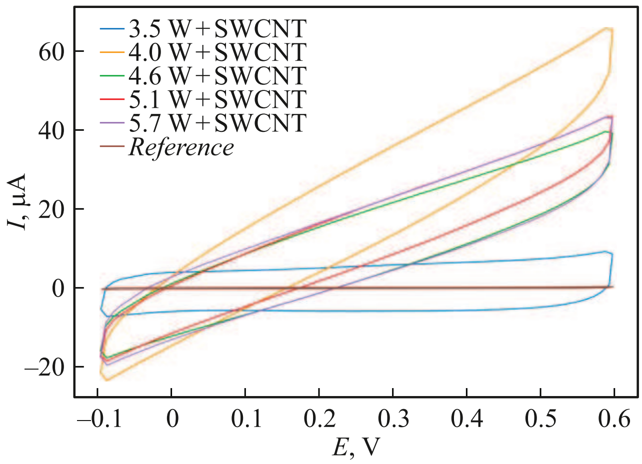

Figure 10. Cyclic voltammograms of the control sample and samples treated with laser radiation of 3.5–5.7 W and coated with SWCNT. Field scan rate — 100 mV/s.

with laser. The obtained curves also have a closed loop without pronounced oxidation-reduction reactions, which also indicates the capacitive nature of the samples. The measured capacitance of the samples is shown in Table 7.

Based on the results obtained, it can be ascertained that the largest area capacitance is expected for the SWCNT-coated sample, irradiated with laser with a power of 4 W. This sample also was featuring a higher stability rate, equal to 98.7 %, compared to the samples exposed to laser radiation of 4.6–5.7 W.

Conclusion

A comprehensive study was carried out for the samples of multiscale nanomaterial structures used in fabrication of passive and active nerve tissue stimulating implantable devices, including morphological, structural, electrical and electrochemical analysis. A process of multiscale structures formation was presented, which included the use of nanosecond laser radiation and the deposition of SWCNT. The results of the surface morphology study showed the formation of a pronounced ordered surface with protruding vertical arrays and recesses. It was confirmed that the height of vertical arrays and recesses changes depending on the power of laser radiation. Thus, within the laser radiation power of 3.5–5.7 W the arrays may be up to 35–72 μm in height. At the same time, the diameter of the arrays did not undergo significant changes, remaining within 40–66 μm for all samples. Also, changing the laser radiation power affected the diameter of the recesses, the size of which was in the range of 11–26 μm. The highest array within the range of 55–72 μm was obtained for the sample irradiated with a 5.7 W laser. SEM method also proved the formation of a uniform SWCNT coating on the samples surface. At the same time, the CNT tubes themselves are not perfectly ordered: the nanotubes assemble into disoriented bundles and form a mesh-like porous structure.

Energy-dispersive X-ray spectroscopy allowed to prove the expected changes in the elemental composition of the surface of samples of multiscale nanomaterial structures used in fabrication of passive and active implantable devices that stimulate nerve tissue. Thus, when using laser radiation in air, an increase in oxide phases was confirmed. At the same time, the sputtering of SWCNT coating led to the expected increase in the carbon content on the surface of the samples.

The conductivity measurements demonstrated repeatability of the obtained results. The effect of laser radiation and SWCNT coating had little effect on the samples conductivity values, which, in turn, were comparable to the control sample, i.e. AISI 321L metal plate, and were equal to (16.0 ± 0.1) S/cm.

During cyclic voltammetry, the expected response was obtained, where it was seen that the control sample did not exhibit catalytic activity in the specified potential range compared to the rest of the samples. In case of the studied samples, it can be seen that the amplitude of the current rises under the influence of increased exposure to laser radiation. The curves themselves were the closed loops, which indicated the capacitive pattern of the samples. The greatest combination of the cycle stability (98.7 %) and area capacity $(125.7\,\mu F/cm^2)$ was demonstrated by a sample irradiated with laser radiation with a power of 4 W and coated with SWCNT. Thus, based on all the obtained data we may estimate the selected method as a promising one for the fabrication of samples of multiscale nanomaterial structures used in the passive and active nerve stimulating implantable devices that involves the use of laser radiation and SWCNT coating, as well as possible commercial application of the materials obtained.

Funding

The study was performed using the equipment of the Core Shared Research Facility „Center for Laser Technologies in Medicine“ with the support of the Ministry of Science and Higher Education of the Russian Federation This study was performed as part of a large research project and funded by the Russian Federation represented by the Ministry of Science and Higher Education of the Russian Federation under Agreement № 075-15-2024-555 dated October 25, 2024.

Conflict of interest

The authors declare that they have no conflict of interest.

References

[1] E. McGlynn, V. Nabaei, E. Ren, G. Galeote-Checa, R. Das, G. Curia, H. Heidari. Adv. Sci., **8** (10), 2002693 (2021). DOI: 10.1002/advs.202002693

[2] P.A. Starr. Front. Neurosci., **12**, 619 (2018). DOI: 10.3389/fnins.2018.00619

[3] A. Burton, S.M. Won, A.K. Sohrabi, T. Stuart, A. Amirhossein, J.U. Kim, Y. Park, A. Gabros, J.A. Rogers, F. Vitale, A.G. Richardson, P. Gutruf. Microsyst. Nanoeng., **7**, 62 (2021). DOI: 10.1038/s41378-021-00294-7

[4] S. Elyahoodayan, W. Jiang, C.D. Lee, X. Shao, G. Weiland, J.J. Whalen III, A. Petrossians, D. Song. Front. Neurosci., **15**, 616063 (2021). DOI: 10.3389/fnins.2021.616063

[5] A.R. Harris, C. Newbold, P. Carter, R. Cowan, G.G. Wallace. Front. Neurosci., **13**, 380 (2019). DOI: 10.3389/fnins.2019.00380

[6] L. Li, C. Jiang, W. Duan, Z. Wang, F. Zhang, C. He, T. Long, L. Li. Microsyst. Nanoeng., **8**, 96 (2022). DOI: 10.1038/s41378-022-00433-8

[7] D. Shuleiko, S. Zabotnov, O. Sokolovskaya, M. Poliakov, L. Volkova, T. Kunkel, E. Kuzmin, P. Danilov, S. Kudryashov, D. Pepelayev, S. Kozyukhin, L. Golovan, P. Kashkarov. Materials, **16** (13), 4524 (2023). DOI: 10.3390/ma16134524

[8] S. Amini, W. Seche, N. May, H. Choi, P. Tavousi, S. Shahbazmohamadi. Sci. Rep., **12**, 13966 (2022). DOI: 10.1038/s41598-022-18161-4

[9] A. Mazzatenta, M. Giugliano, S. Campidelli, L. Gambazzi, L. Businaro, H. Markram, M. Prato, L. Ballerini. J. Neurosci., **27** (26), 6931 (2007). DOI: 10.1523/JNEUROSCI.1051-07.2007

[10] N. Burblies, J. Schulze, H.C. Schwarz, K. Kranz, D. Motz, C. Vogt, T. Lenarz, A. Warnecke, P. Behrens. PLoS One, **11** (7), e0158571 (2016). DOI: 10.1371/journal.pone.0158571

[11] K. Foremny, W.S. Konerding, A. Behrens, P. Baumhoff, U.P. Froriep, A. Kral, T. Doll. Nanomaterials, **11** (4), 1029 (2021). DOI: 10.3390/nano11041029

[12] T. Murakami, N. Yada, S. Yoshida. Micromachines, **15** (5), 650 (2024). DOI: 10.3390/mi15050650

[13] N.P. Pampaloni, M. Giugliano, D. Scaini, L. Ballerini, R. Rauti. Front. Neurosci., **12**, 953 (2019). DOI: 10.3389/fnins.2018.00953

[14] N. Elgrishi, K.J. Rountree, B.D. McCarthy, E.S. Rountree, T.T. Eisenhart, J.L. Dempsey. J. Chem. Educ., **95** (2), 197 (2018). DOI: 10.1021/acs.jchemed.7b00361

[15] G. Schmidl, G. Jia, A. Gawlik, J. Kreusch, F. Schmidl, J. Dellith, A. Dathe, Z.-H. Lin, J.-S. Huang, J. Plentz. Sci. Rep., **8**, 11283 (2018). DOI: 10.1038/s41598-018-29661-7

[16] A. Kunisaki, A. Kodama, M. Ishikawa, T. Ueda, M.D. Lima, T. Kondo, N. Adachi. Sci. Rep., **13** (1), 21799 (2023). DOI: 10.1038/s41598-023-48534-2

[17] A. Shar, A. Shar, D. Joung. Front. Bioeng. Biotechnol., **11**, 1299166 (2023). DOI: 10.3389/fbioe.2023.1299166

Translated by T.Zorina